August 27-31, 2023
FLORENCE - ITALY
ICWE 16
16th International Conference on Wind Engineering

Numerical simulation of vehicle-induced loads on fully enclosed sound barrier

Yaoheng Feng [1], Zhiwen Liu [2*], Zhengqing Chen [3]

[1] *Hunan Prov. Key Laboratory for Wind & Bridge Eng., Hunan University, Changsha, China, fyh2019@126.com*
[2*] *Hunan Prov. Key Laboratory for Wind & Bridge Eng., Hunan University, Changsha, China, zhiwenliu@hnu.edu.cn*
[3] *Hunan Prov. Key Laboratory for Wind & Bridge Eng., Hunan University, Changsha, China, zqchen@hnu.edu.cn*

ABSTRACT:

In this study, the vehicle-induced loads on fully enclosed sound barriers are investigated via computational fluid dynamic (CFD) method for vehicles pass in different lanes in the same direction and opposite direction, respectively. The numerical simulation method for vehicle-induced loads on sound barriers based on sliding-mesh technique is proposed in this study, and the validation of the proposed method is conducted for the free-standing vertical sound barrier. Furthermore, the vehicle-induced loads on enclosed is simulated by applying the proposed numerical method. The results show that the vehicle-induced loads on the fully enclosed sound barriers near the vehicles all present the law of "positive-negative-negative-positive". Moreover, when the vehicle pass through the sound barriers in the same direction and opposite direction, the vehicle-induced pressure loads on the fully enclosed sound barriers increases gradually with the increase of the number of vehicles. Furthermore, the vehicle-induced pressure loads on the fully enclosed sound barriers are higher than that on the free-standing vertical sound barriers.

Keywords: Fully enclosed sound barrier, vehicle-induced loads, computational fluid dynamics (CFD)

1. INSTRUCTIONS

With the development of traffic infrastructure, the traffic noise has gradually become an important issue affecting people's lives. Setting free-standing vertical or fully enclosed sound barriers on both sides of roads or bridges is one of the important measures to reduce the traffic noise. However, the passing vehicle may cause an overpressure on the sound barrier at the front of the vehicle, and cause a suction pressure on the sound barrier at the leading edge of the vehicle. Quinn et al. (2001) investigated the vehicle-induced loads on flat plates, and the experimental results show that loading on road signs can be separated into wind loads and vehicle-induced loads. Furthermore they suggested the effect of vehicle to sign separation distance is to be an inverse square relationship. Sanz-Andres et al. (2003) present a mathematical model for the vehicle-induced load on a flat sign panel, able to explain the main characteristics of the phenomenon. Lichtneger and Ruck (2018) performed full scale experiments for different vehicle types, and provided a big database for the proper quantification of vehicle-induced pressure loads on roadside walls as a function of vehicle types, vehicle velocities and the passing

distance. Soper et al. (2019) carried out on-site measurement of railway vertical sound barriers, found that the wind pressure of the sound barrier is closely related to the type of trains.

Overall, most of the previous studies focused on the field measurement and CFD numerical simulation of vehicle-induced loads on vertical sound barriers, and some researchers studied the railway enclosed sound barriers, however, the investigations on vehicle-induced loads on enclosed sound barriers are relatively few. In this study, the vehicle-induced loads on fully enclosed sound barriers are investigated via computational fluid dynamic (CFD) method for vehicles pass in different lanes in the same direction and opposite direction, respectively.

2. NUMERICAL SIMULATION

2.1. Computational model

The fully enclosed sound barrier on a practical bridge with two-way four lanes is selected as background, and the width (B_s), height (H_s) and length (L_s) of the fully enclosed sound barrier is 16.24m, 7.3m and 52.4m, respectively. Moreover, a bus is selected as the vehicle model due to the large vehicle-induced loads on sound barriers, and the width, height and length of the vehicle model is 2.55m (L_v), 3.695m (B_v) and 13.1m (H_v), respectively. Figure 1(a) shows the fully enclosed sound barrier and lanes on the road.

2.2. Computational Domain and Boundary Conditions

Considering requirement of the blocking ratio, the three-dimensional computational domain is selected as shown in Figure 1(b). The computational domain is divided into static domain and dynamic domain, and the dynamic domain includes the vehicle model. The static domain includes the sound barrier model. The length, width and height of the static domain is $10L_v$, $30B_v$ and $10H_v$, respectively. Moreover, the length, width and height of the dynamic domain is $40L_v$, $1.2B_v$ and $1.1H_v$, respectively. The boundary conditions are shown in Figure 1(b). The structured grid is used to mesh the computational domain, and the mesh of the bus and sound barrier is shown in Figure 1(c) and (d).

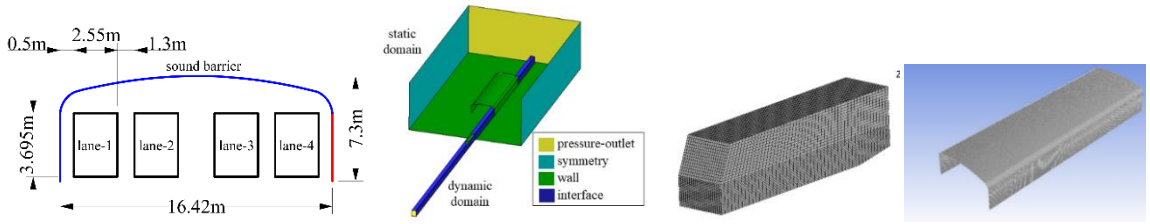

(a) (b) (c) (d)

Figure 1 Fully enclosed sound barrier, computational domain and mesh of bus and sound barrier: (a) Fully enclosed sound barrier and lanes, (b) computational domain and boundaries, (c) mesh of bus, and (d) mesh of sound barrier.

2.3. Turbulence model and measuring points

The standard k-ε model is used to model the turbulent flow, and the sliding-mesh technique is applied to simulate the moving vehicle. The time step is 0.002 s. The pressure measured points are arranged in the mid-span section of the fully enclosed sound barrier as shown in the Figure 2. As shown in Table 1, eight cases are simulated to study the effects of lanes and directions on vehicle-induced loads on sound barriers.

Table 1. Main parameters of the numerical simulation cases

Case	Vehicle numbers	Vehicle on lanes	Sound barrier type	Vehicle speed (km/h)	Number of grids
Case-1	1	Lane-4	free-standing vertical sound barrier	90	3×10^6
Case-2	1	Lane-4	free-standing vertical sound barrier	90	5×10^6
Case-3	1	Lane-4	free-standing vertical sound barrier	90	8×10^6
Case-4	1	Lane-4	free-standing vertical sound barrier	120	5×10^6
Case-5	1	Lane-4	Fully enclosed sound barrier	120	5×10^6
Case-6	2	Lane-3, Lane-4	Fully enclosed sound barrier	120	5×10^6
Case-7	2	Lane-1, Lane-4	Fully enclosed sound barrier	120	5×10^6
Case-8	4	Lane1~Lane4	Fully enclosed sound barrier	120	5.5×10^6

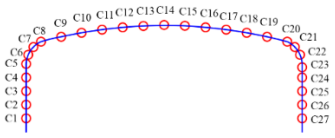

Figure 2. Measuring point layout

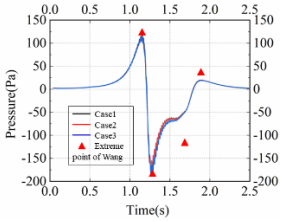

Figure 3. Numerical Simulation Method Validation

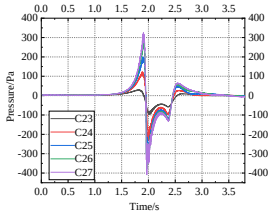

Figure 4. Vehicle-induced pressure on free-standing vertical sound barrier for case-4

3. CALCULATION RESULTS AND DISCUSSION

3.1. Free-standing vertical sound barrier

In order to verify the numerical simulation method, this section reproduces the computational fluid dynamics conditions in Wang's research(case-1~case-3). The comparison of calculation results is shown in Figure 3. It can be seen from Figure 3 that the maximum absolute value of wind pressure calculated by three different cases are almost consistent with that in Wang's research, which proves that the numerical simulation method used in the study is accurate and reliable (Wang et al., 2013). Figure 4 shows the **v**ehicle-induced pressure on free-standing vertical sound barrier for case-4. The free-standing vertical sound barrier is show in red in Figure 1(a). In figure 4, the maximum absolute value of wind pressure is 408 Pa.

3.2. Fully enclosed sound barrier

Figure 5 and Figure 6 show the results of case-5 and case-6. Due to the limited length of the abstract, the results of case-7 and case-8 are supplemented in the full paper.

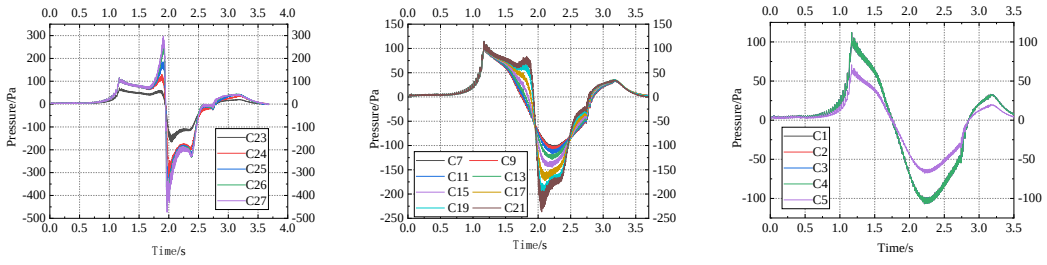

(a) (b) (c)

Figure 5. Vehicle-induced pressure on fully enclosed sound barrier for case-5: (a) C23~C27, (b) C7~C21, (c) C1~C5.

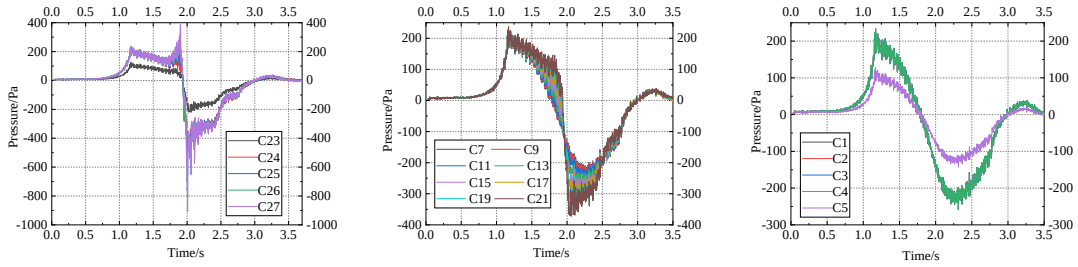

(a) (b) (c)

Figure 6. Vehicle-induced pressure on fully enclosed sound barrier for case-6: (a) C23~C27, (b) C7~C21, (c) C1~C5.

It can be seen from Figure 5(a) that the vehicle-induced loads on the fully enclosed sound barrier is similar to that on the free-standing vertical sound barrier, both showing the law of "positive-negative-negative-positive". The maximum absolute value of wind pressure is 473 Pa. Comparing with the free-standing vertical sound barrier, the vehicle-induced pressure loads on the fully enclosed sound barriers is higher than that on the free-standing vertical sound barriers. It can be seen from Figure 5(b) and Figure 5(c) that the greater the distance between the measuring point and the vehicle, the smaller the pulsating wind pressure. Comparing Figure 6 with Figure 5, the vehicle-induced loads increases as the number of vehicles increases.

4. CONCLUSIONS

(1) When the vehicle passes through the sound barriers, the vehicle-induced pressure loads at the measuring points near the vehicle shows the law of "positive-negative-negative-positive".

(2) In a fully enclosed sound barrier, the number of vehicles has a great influence on the vehicle-induced pressure loads on the sound barriers when the vehicles pass in the same direction or meet in opposite directions.

(3) The vehicle-induced pressure loads on the fully enclosed sound barriers is higher than that on the free-standing vertical sound barriers.

ACKNOWLEDGEMENTS

This research was financially supported by the National Natural Science Foundation of China (Grant No. 52178475, 51778225), for which the authors are grateful.

REFERENCES

Quinn A.D., Baker C. J., Wright N.G., 2001. Wind and vehicle induced forces on flat plates – Part 2: vehicle induced force, Journal of Wind Engineering and Industrial Aerodynamics 89, 831-847.

Sanz-Andres A., Santiago-Prowald J., Baker C., Quinn A., 2003. Vehicle-induced loads on traffic sign panels, Journal of Wind Engineering and Industrial Aerodynamics 91, 925-942.

Lichtneger P., Ruck B., 2018. Full scale experiments on vehicle induced transient pressure loads on roadside walls, Journal of Wind Engineering & Industrial Aerodynamics 174, 451-457.

Soper, D., Gillmeier, S., Baker, C., Morgan, T., & Vojnovic, L., 2019. Aerodynamic forces on railway acoustic barriers. Journal of Wind Engineering and Industrial Aerodynamics 191, 266-278.

Wang, D., Wang, B., & Chen, A., 2013. Vehicle-induced aerodynamic loads on highway sound barriers part2: numerical and theoretical investigation. Wind and Structures 17, 479-494.